Available online at www.sciencedirect.com
SCIENCE DIRECT®

Journal of the European Ceramic Society 24 (2004) 2749–2761

www.elsevier.com/locate/jeurceramsoc

Correlation between densification rate and microstructural evolution for pure alpha alumina

D. Lance, F. Valdivieso, P. Goeuriot*

Département Céramiques Spéciales, UMR CNRS 5146, Ecole Nationale Supérieure des Mines de Saint-Etienne, 158 cours Fauriel, 42023 Saint-Etienne cedex 2, France

Received 14 February 2003; received in revised form 20 August 2003; accepted 6 September 2003

Abstract

Correlation between microstructural evolution and macroscopic measurements has been investigated on pure alpha alumina under non-isothermal conditions. The densification of different as-received and milled powders of alumina has been monitored during sintering. Densification rate curves as a function of relative density are sensitive to microstructure, such as initial parameters of microstructure (agglomeration, pore size, heterogeneities), and heating schedule (thermal pre-treatment, heating rate). Densification rate curves can be correlated with microstructural evolution during overall sintering and are expected to be a good help to choose raw materials.

Keywords: Al_2O_3; Dilatometry; Microstructure-final; Microstructure-prefiring; Sintering

1. Introduction

Sintering is a complicated process that involves microstructural evolution through the action of several different mechanisms. Sintering kinetics in ceramics has been widely studied in the literature and is known to be in direct relationship with the microstructure. It is therefore desirable to monitor microstructural evolution during the entire course of densification.

Non-isothermal method is well suitable for such a study, since it requires much less experimental work and time than isothermal method. Moreover, it is well known that constant heating rate experiments are used to estimate the activation energy and the dominant diffusion mechanism in the intermediate stage of sintering.[1–3] Several authors reported that, in this stage, sintering kinetics of submicron alumina is believed to be controlled by grain boundary diffusion.[4,5]

Furthermore, sintering is traditionally viewed in terms of three distinct stages (initial, intermediate and final) and most of the models have focused on a specific stage. Hansen et al.[6] have then proposed a generalized model with a single equation of shrinkage rate which quantifies sintering as a continuous process from the beginning to the end. If there exists only one dominant diffusion mechanism in the sintering process, Su and Johnson[7] have simplified the foregoing equation and converted it to the instantaneous densification rate by:

$$\frac{1}{\rho}\frac{\mathrm{d}\rho}{\mathrm{d}t} = 3\frac{\Omega\gamma D_0}{k_\mathrm{B}}\frac{\Gamma(\rho)}{G^n}\frac{\mathrm{e}^{-Q/RT}}{T} \quad (1)$$

where ρ is relative density; t is time; Ω is the atomic volume; γ is the surface energy; D_0 is the pre-exponential coefficient diffusion; k_B is the Boltzmann constant; $\Gamma(\rho)$ is function only of microstructural features and geometry parameters;[6] G is the mean grain size; Q is the apparent activation energy; R is the gas constant; T is the absolute temperature. For volume diffusion, $D_0 = (D_\mathrm{V})_0$ and $n = 3$; for grain boundary diffusion, $D_0 = (\delta D_\mathrm{b})_0$ where δ is grain boundary thickness and $n = 4$. In writing Eq. (1), it is assumed that Γ and G values are functions only of density. It is therefore possible to separate terms related to the microstructural and materials properties and terms related to heating schedule in Eq. (1) as follows:

* Corresponding author. Tel.: +33-477-420-019; fax: +33-477-420-249.
E-mail address: pgoeurio@emse.fr (P. Goeuriot).

0955-2219/$ - see front matter © 2003 Elsevier Ltd. All rights reserved.
doi:10.1016/j.jeurceramsoc.2003.09.010

$$\frac{1}{\rho}\frac{d\rho}{dt} = \dot{\rho}_i = A^* F(\rho)^* \theta(T) \quad (2)$$

Here $\dot{\rho}_i$ is the instantaneous densification rate; A includes all constants; $F(\rho)$ is equal to $\Gamma(\rho)/G(\rho)^n$ and is function only of density and $\theta(T)$ is function only of temperature.

Thus, $F(\rho)$ is considered to be dependent on microstructural geometry. Hansen et al.[6] have described $F(\rho)$ with sintering parameters $\Gamma(\rho)$, which relate the driving force, mean diffusion distance, and other microstructural geometric features on the grain size. They suggested that $F(\rho)$ either increases or decreases slightly with density. $F(\rho)$ has also been formulated by Chen et al.[8] but their expression is only valid for a re-packing mechanism in porous materials when $\rho < 0.63$.

In the final-stage of sintering, grain growth accompanies an increased pore separation, and thus an increase in the diffusion path length, and the densification rate should decrease with density. Several authors have observed that this decrease is exponential with density for "frozen" microstructures[9] or for compacts that sinter under low uniaxial stress.[10] Other authors have proposed that the drop in densification rate takes place when the pores break away from the boundary, so that they could only be eliminated by the slower diffusion process.[11,12] Several studies[13–15] showed that the number of pores per unit volume, has a major influence on the densification kinetics. Therefore, increasing the number of pores per unit volume would enhance densification rate at constant ρ and G, and narrowing the pore size distribution would inhibit grain growth and increase densification rate indirectly. In addition, Mayo[16] showed that densification rate is inversely proportional to the pore size for nanocrystalline zirconia.

Furthermore, many other initial parameters of green sample have a great influence on densification rate, such as green density,[10,16,17] particle size distribution,[18,19] heterogeneity like aggregates[20–22] or large porosity,[23] and the fabrication history of powder.[24] Microstructural evolution is not only predetermined by the initial particle and pore size distributions, but heating schedule can significantly affect final microstructure.[25–27] Hence, the effect of heating rate on densification rate has been measured,[7,28,29] and densification rate increases almost linearly with the heating rate at a given temperature.

In this study, the correlation between densification rate curves as a function of relative density and observed microstructural evolution of pure alpha alumina was investigated under non-isothermal conditions from the beginning to the end of the sintering process. The influence of green state and heating schedule on $\dot{\rho}_i$ of alumina is also discussed.

2. Experimental procedure

2.1. Materials, processing and sintering conditions

Three high purity undoped alpha alumina powders (Baikowski Chimie, France), denoted A, B and C, with a submicron size were used in this study. The main features of the as-received powders are summarized in Table 1. The powders were dispersed in deionized water at pH 10 using a polyacrylic acid with an average molecular weight of 2000 (Acros Organics, USA). The amount of dispersant was optimized by viscosimetry to ensure a good dispersion of the slurry. The resulting slips with a solid loading of 60 wt.% were also ultrasonically dispersed. Some of the suspensions were attrition milled in a laboratory batch mill (Netzsch, Germany) with 1.25-mm zirconia balls. The attrition milling was performed at 1500 rpm for 1 h. The slurries were then deaired under vacuum to remove gas bubbles. The particle size distributions of the final suspensions were measured using an X-ray disc centrifuge (Model Bi-XDC, Brookhaven, USA). The materials will be denoted respectively, a-A, a-B and a-C for the as-received powders, and m-A, m-B and m-C for the milled powders. Another samples have been attrition milled under different conditions, i.e. performed on C powder at 830 rpm for 1 h with 2 mm zirconia balls. The previous samples are denoted m-C2.

The slurries were poured into a silicon mould with 10-mm height and 10-mm diameter cylindrical holes, placed onto a gypsum mould. A 0.2 μm cellulose filter, between slurry and gypsum, was used to prevent contamination and to limit the water absorption rate of gypsum. After demoulding, the cast samples were dried

Table 1
Mean features of the alumina powders used in the present study

Powder	Specific surface area (m^2/g)	Mean particle size (μm)	Alpha content (%)	Chemical analysis (ppm)					
				Na	K	Fe	Ca	Si	Mg
A	6.2	0.48	100	11	22	4	2	24	1
B	10.0	0.25	100	7	18	5	2	16	2
C	15.5	0.18	100	40	21	4	30	132	9

at room temperature and then air calcined at 600 °C for 1 h to remove organic dispersants.

Sintering was performed up to 1550 °C under non-isothermal conditions in air with various heating rates, and cooled to room temperature. Final densities were measured in water by Archimedes method. The density of theoretical fully dense alumina was the one of pure alumina (3.987 g/cm^3) corrected for zirconia contamination measured by X-ray fluorescence. Microstructures were observed by field emission scanning electron microscopy (Model 6500F, JEOL, Japan) on polished and thermally etched sections. Grain sizes of sintered samples were determined by the intercept method.

Three green samples from C powder with different agglomeration states are illustrated on Figs. 1–3, respectively for a-C, m-C and m-C2 samples.

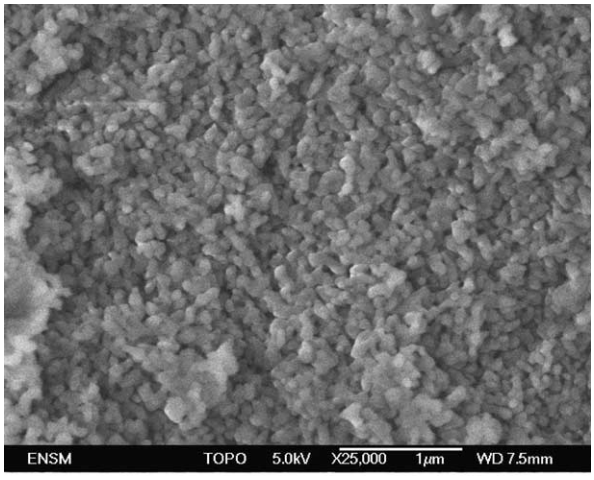

Fig. 1. SEM micrograph of a-C green sample.

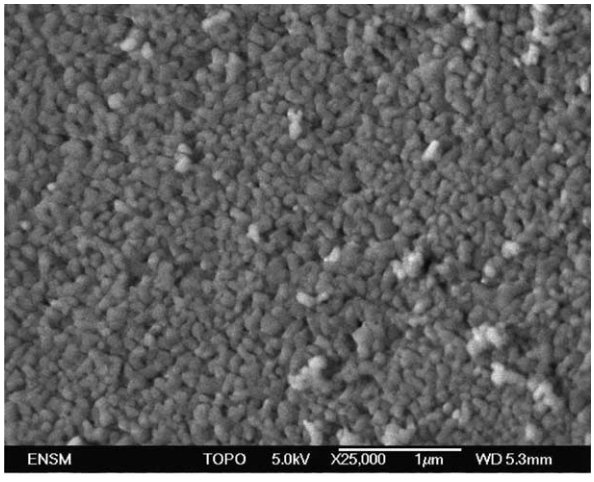

Fig. 2. SEM micrograph of m-C green sample.

2.2. Dilatometric characterization

The shrinkage as a function of time and temperature was followed by dilatometry (Setsys from SETARAM, France). Thermal expansion of the measurement device was calibrated by a reference run with a fully dense specimen of alumina of the same dimensions as the green specimens. The axial and radial measurements of final shrinkage after cooling were compared to check the isotropy of shrinkage strain. The shrinkage was anisotropic, and radial shrinkage was considered proportional to axial shrinkage. The time dependent relative density was calculated from the following expression:

$$\rho(t) = \frac{\left(1+\frac{(L_f - L_0)}{L_0}\right)\left(1+\frac{(\phi_f - \phi_0)}{\phi_0}\right)^2}{\left(1+\frac{\Delta L(t)}{L_0}\right)\left(1+\alpha\frac{\Delta L(t)}{L_0}\right)^2}\rho_f \quad (3)$$

Here L_f and L_0 are, respectively, the final and the initial length of the specimen; ϕ_f and ϕ_0 are, respectively, the final and the initial mean diameter of the specimen; ΔL(t) is the change in length of the specimen; ρ_f is the final relative density; and α is the anisotropic shrinkage factor defined by:

$$\alpha = \frac{(\phi_f - \phi_0)}{(L_f - L_0)}\frac{L_0}{\phi_0} \quad (4)$$

Relative density is thereby calculated with Eq. (3) from final density and dilatometric measurements.

3. Results

3.1. Influence of green state on densification rate curves

3.1.1. Influence of attrition milling

Table 2 reports the particle size distributions of all the powders in suspension and the features of green samples after slip casting. Attrition milling decreases greatly d_{90} values, moderately d_{50} values and slightly d_{10} values for all powders. Most of the agglomerates have been broken up, and the particle size distributions become finer. Mean pore sizes also decrease and attrition milling enhances the green density of slip-cast bodies. The m-C sample has the finer grain size and will be used as a reference for the rest of the study.

The foregoing results are confirmed by the microstructures of a-C and m-C green samples, respectively reported in Figs. 1 and 2. Thus, the microstructure of a-C sample is heterogeneous with large agglomerates. The one of m-C sample is homogeneous and agglomerate-free with small pores; the observed particles are well packed and their size is almost monomodal.

Non-isothermal dilatometric analyses are commonly reported as shrinkage rate or densification rate versus temperature or relative density. Densification rate and relative density seem to be more suitable for the description of microstructure than shrinkage rate and temperature. Actually, shrinkage rate reports densification in only one dimension, whereas $\dot{\rho}_i$ reports densification in three dimensions. Therefore, in the present study, sintering kinetics will be plotted with $\dot{\rho}_i$ as a function of ρ, calculated from Eq. (3).

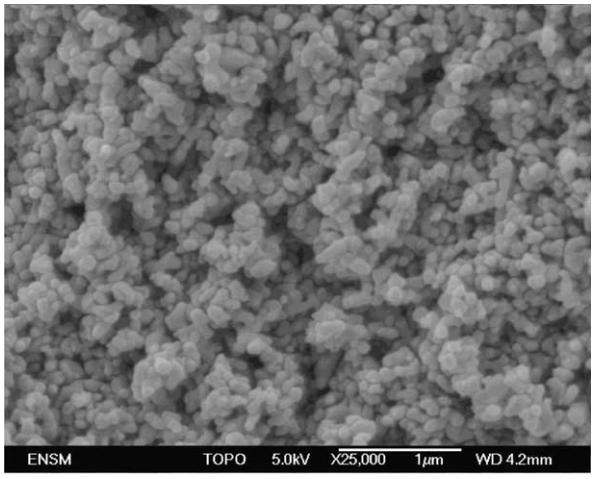

Fig. 3. SEM micrograph of m-C2 green sample.

Fig. 4 shows this kind of curve for a-C and m-C samples at the heating rate of 5 °C/min. The instantaneous densification rate increases from green state to the intermediate stage of sintering, undergoes a maximum and then decreases with increasing density. At the very beginning of sintering, $\dot{\rho}_i = f(\rho)$ plots increase linearly. The linear increasing part of $\dot{\rho}_i$ is much longer for m-C sample, whereas for a-C sample, there is a break in the increasing part of $\dot{\rho}_i$ with a second slope of a lower value. Actually, between green density and a relative density of about 70%, $\dot{\rho}_i$ increases according to only one slope for m-C sample and according to two slopes for a-C sample. Maximum $\dot{\rho}_i$ occurs at a relative density of about 70% for a-C sample and is shifted to 82% density for m-C sample. Note that the value of maximum $\dot{\rho}_i$ is greater for m-C sample.

Table 2
Features of green samples after slip casting

Materials	Particle size distribution (nm)			Mean radius of pore size (nm)	Pore size/grain size ratio	Green density (%)
	d_{10}	d_{50}	d_{90}			
a-A	290	484	1568	69	0.28	45.4
a-B	160	247	530	36	0.29	55.6
a-C	127	176	330	29	0.33	48.7
m-A	153	261	430	34	0.26	62.3
m-B	130	199	350	25	0.25	62.1
m-C	89	129	214	18	0.28	58.0

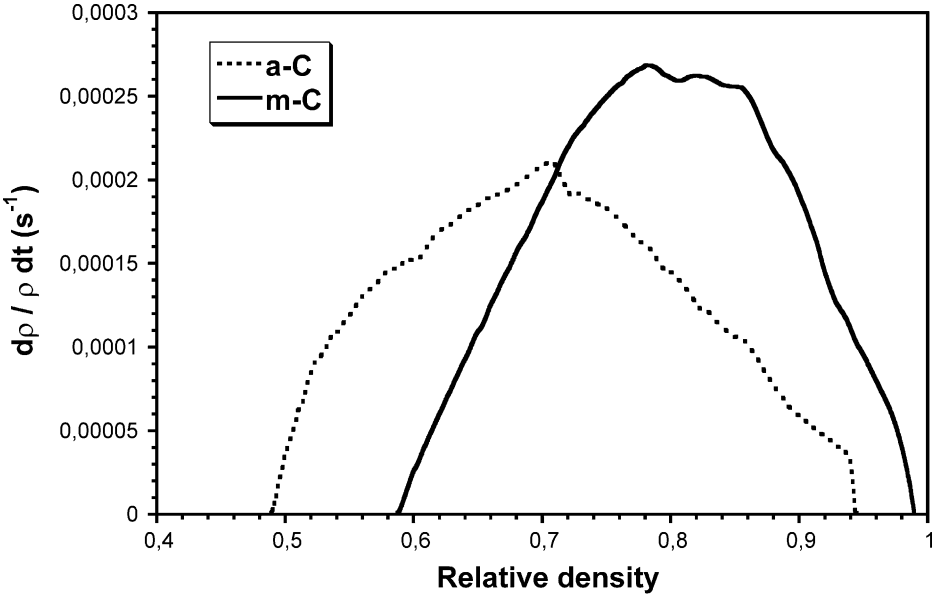

Fig. 4. Densification rate as a function of relative density for a-C and m-C samples heated at 5 °C/min up to 1550 °C.

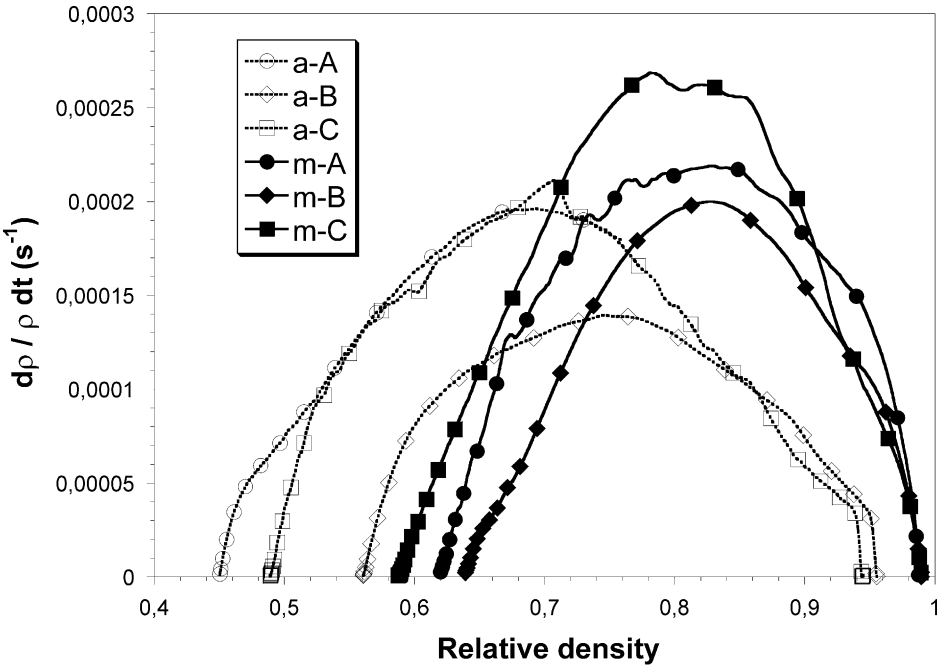

Fig. 5. Densification rate as a function of relative density for all samples heated at 5 °C/min up to 1550 °C.

Fig. 5 reports $\dot{\rho}_i$ as a function of ρ for all samples heated at 5 °C/min up to 1550 °C. For as-received samples, the increasing part of $\dot{\rho}_i$ shows several segments. For milled samples, there is only one slope of $\dot{\rho}_i$ at the beginning of sintering, except for m-B sample where a small shoulder appears. Furthermore, densification is not complete for as-received samples at the end of heating, since such a heating schedule is not sufficient to achieve almost full density, as it does for milled samples.

3.1.2. Influence of green density

It is interesting to point out that green densities calculated with Eq. (3) at $t=0$ and reported in Fig. 5 are in good agreement with those geometrically measured and reported in Table 2. Thus, all samples show different green densities. Nevertheless, at the very beginning of sintering, i.e. in the first 2% of densification, slopes of $\dot{\rho}_i$ for all samples are approximately parallel on Fig. 5. Accordingly, the slope of $\dot{\rho}_i$, at the very beginning of sintering, is independent of green density whatever the agglomeration state of the alumina powders from the present work.

3.1.3. Influence of heterogeneities

The previous m-C samples have been compared to m-C2 samples that have been attrition milled under different conditions. The microstructure of m-C2 sample in Fig. 3 is not as homogeneous as the one of m-C sample in Fig. 2. Actually, the attrition milling for m-C2 sample has not been efficient to break up most of the agglomerates, and therefore an heterogeneous powder packing can be observed in Fig. 3. Furthermore, three m-C2 green samples, denoted m-C2a, m-C2b and m-C2c, with approximately the same green density of about 57%, have been sintered at 5 °C/min. Fig. 6 shows the evolution of $\dot{\rho}_i$ for the foregoing samples. In the first part of sintering, the evolution of $\dot{\rho}_i$ is approximately equivalent for the three samples, with small fluctuations of $\dot{\rho}_i$ for m-C2b and m-C2c samples. However, at the end of sintering for density above 90%, the evolution of $\dot{\rho}_i$ is completely different. The decrease of $\dot{\rho}_i$ is regular for m-C2a sample, follows a shoulder for m-C2b sample and undergoes a plateau of densification between 93 and 98% of relative density for m-C2c sample. The final sintered microstructures for m-C2a, m-C2b and m-C2c are respectively illustrated on Figs. 7–9. The microstructure of m-C2a sample is fine and rather homogeneous. The one of m-C2b shows the beginning of abnormal growth for a few grains. The one of m-C2c is heterogeneous and shows great abnormal grain growth (AGG). Furthermore, for the last sample, heating was performed at higher temperature up to 1600 °C. In fact, dilatometric analysis shows that densification only occurs up to about 1550 °C, whereas there is no shrinkage beyond 1550 °C and AGG is dramatically enhanced between 1550 and 1600 °C. Although m-C2a, m-C2b and m-C2c samples have approximately the same green density, their powder packing are heterogeneous, which leads to different sintering behaviors.

Heterogeneity in milled green sample, such as an heterogeneous powder packing arising from an inefficient attrition milling, has a slight influence on the beginning

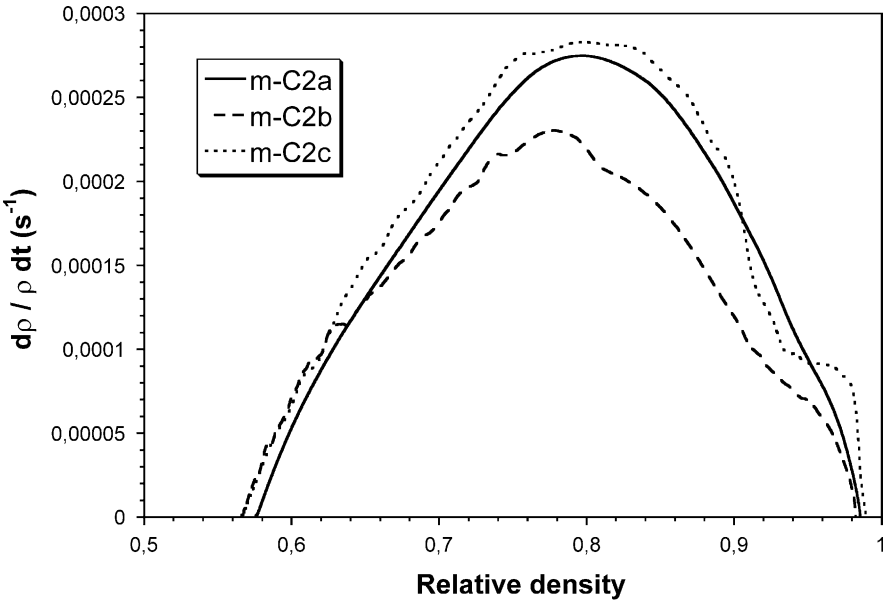

Fig. 6. Densification rate as a function of relative density for m-C2a, m-C2b and m-C2c samples heated at 5 °C/min, up to 1500 °C for m-C2a and m-C2b samples and up to 1600 °C for m-C2c sample.

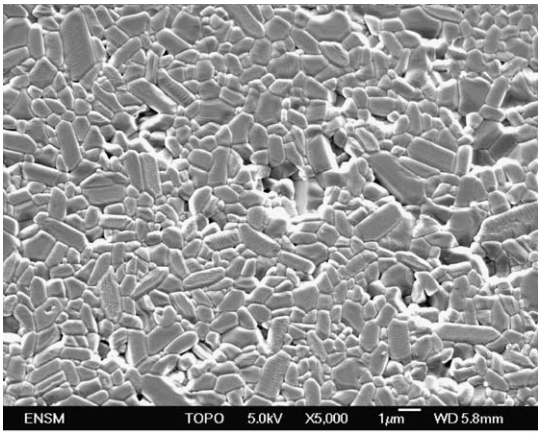

Fig. 7. SEM micrograph of m-C2a sample sintered up to 1550 °C at 5 °C/min. Final density is 99.0%.

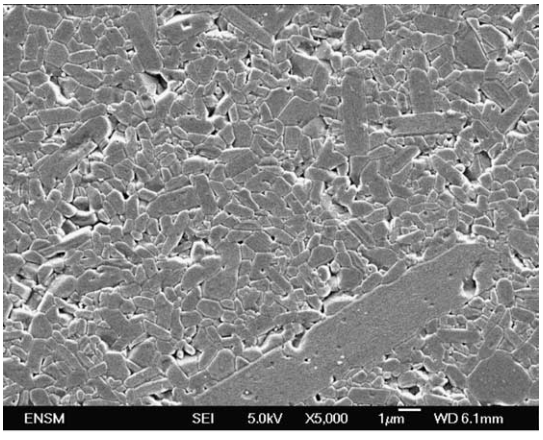

Fig. 8. SEM micrograph of m-C2b sample sintered up to 1550 °C at 5 °C/min. Final density is 99.2%.

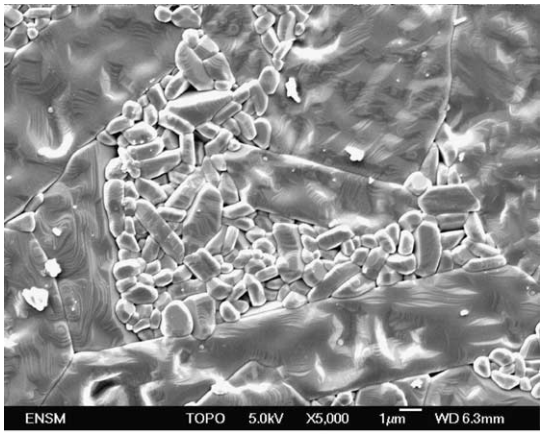

Fig. 9. SEM micrograph of m-C2c sample sintered up to 1600 °C at 5 °C/min. Final density is 99.2%.

of densification resulting in fluctuations in $\dot{\rho}_i$. Nevertheless, it has a great effect on densification in the final stage of sintering and on final microstructure.

3.2. Influence of heating schedule on densification rate curves

3.2.1. Influence of pre-heating treatment

The m-B green sample shows a small shoulder in the very beginning of densification. It was heated up to 900 °C during 68 h in air. Fig. 10 reports densification behavior up to 1550 °C at 5 °C/min of m-B sample with and without pre-heating treatment. The shoulder in the very beginning of densification has disappeared with pre-heating. Densification behavior is approximately the same for both samples after the foregoing event. The two curves intersect at the relative density of about 97%

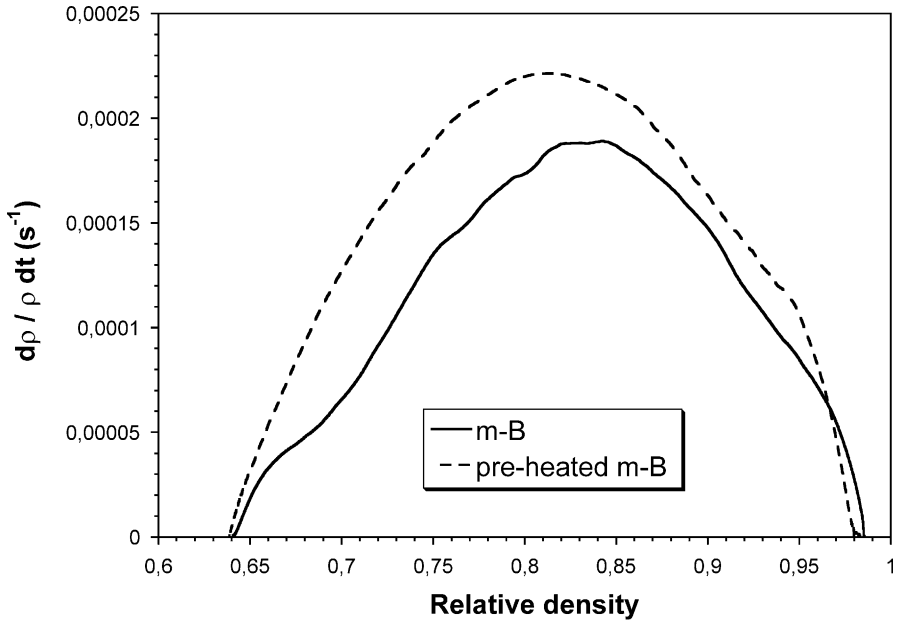

Fig. 10. Densification rate as a function of relative density for m-B sample heated at 5 °C/min up to 1550 °C with and without pre-heating treatment.

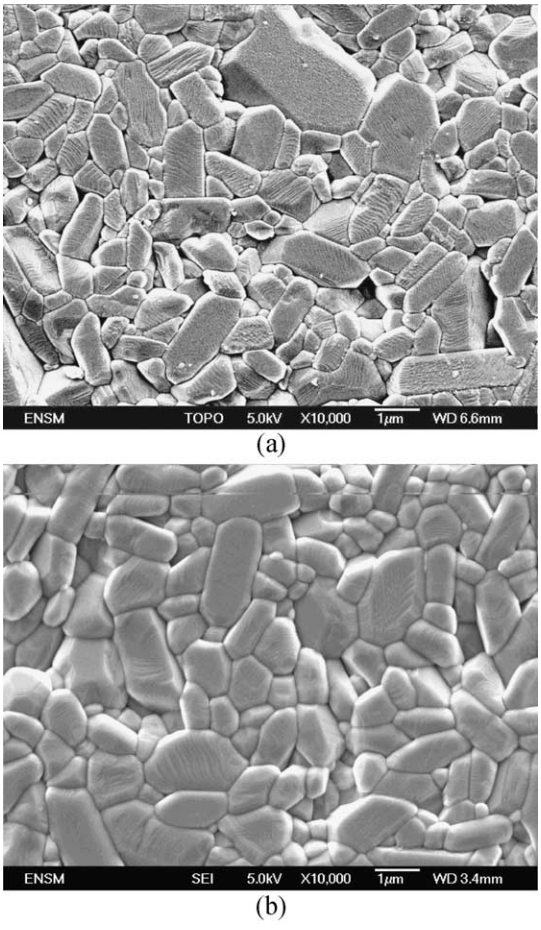

Fig. 11. SEM micrograph of m-B sample sintered up to 1550 °C at 5 °C/min without pre-treatment (a) and pre-heated up to 900 °C during 68 h in air (b).

with a more important slowing down of $\dot{\rho}_i$ for pre-heated sample. Final microstructures of both samples are shown in Fig. 11(a) and (b). The microstructure of pre-heated sample is more homogeneous and slightly coarser. Thus, the grain size distribution of sample without pre-heating is large, whereas pre-heating induces a narrower grain size distribution.

Pre-heating treatment has only an effect on the initial shoulder of densification and seems to homogenize final microstructure. This in a good agreement with the work of Sato and Carry[30] that showed the disappearance of the shoulder of densification with thermal pre-treatment, resulting in coarser and homogeneous final microstructure.

3.2.2. Influence of heating rate

The effect of heating rate was investigated on m-C sample. Fig. 12 reports $\dot{\rho}_i$ versus ρ with heating rates of 2, 5 and 10 °C/min up to 1550 °C. $\dot{\rho}_i$ increases linearly with ρ for the 3 heating rates in the first part of densification. Maximum densification rates occur at the same relative density of about 80%. If relative density is differentiated with respect to temperature, i.e. $d\rho/\rho dT$ versus ρ as shown in Fig. 13, all plots fit a common curve. At a constant value of ρ, there is only one value of $d\rho/\rho dT$, whatever the value of constant heating rate. Maximum $d\rho/\rho dT$ also occurs at 80% and is independent of heating rate. The microstructure of m-C sample heated at 5 °C/min up to 80% is observed on Fig. 14 and is similar to those obtained at 2 and 10 °C/min up to the same density. Note that microstructure is composed of porous areas and dense areas, where some grains have

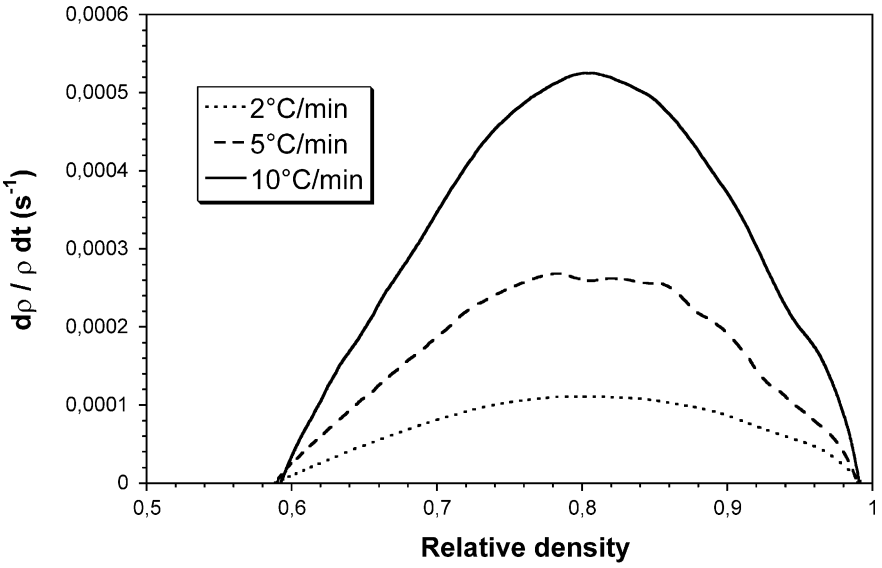

Fig. 12. Densification rate as a function of relative density for m-C samples with heating rates of 2, 5 and 10 °C/min up to 1550 °C.

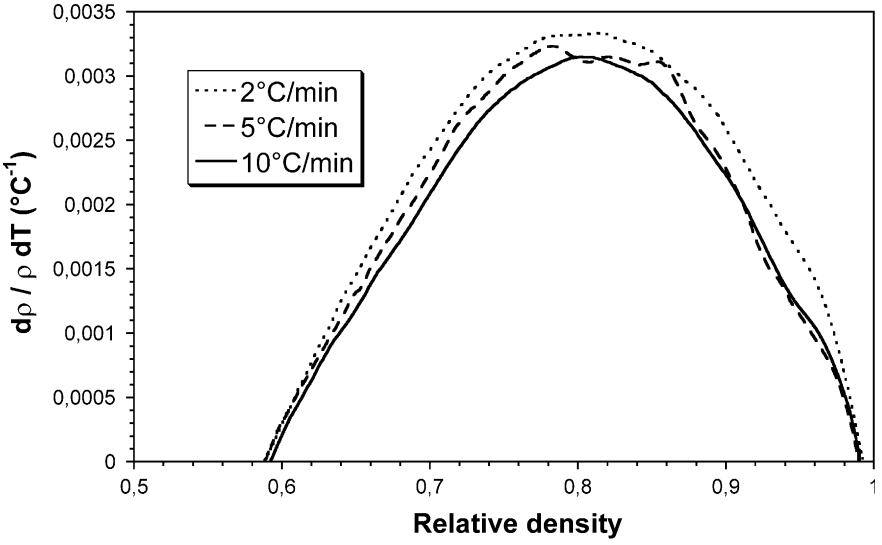

Fig. 13. $d\rho/\rho dT$ as a function of relative density for m-C samples with heating rates of 2, 5 and 10 °C/min up to 1550 °C.

already sintered and are bordered by linear grain boundaries.

3.2.3. *Influence of variation of heating rate*

In the case of attrition milled samples, $\dot{\rho}_i$ increases linearly with relative density up to about 75%. It is possible to extend the linear part of the curves by altering the heating schedule. Thus, seeing that the increase of $\dot{\rho}_i$ is not linear anymore, heating rate is slightly increased for a few minutes and then decreased to its initial value. Note that the present work tries to continue the linearity of $\dot{\rho}_i$ and not to keep $\dot{\rho}_i$ constant, like in rate controlled sintering.[25,31] Fig. 15 plots $\dot{\rho}_i$ versus density for m-C2 sample at various constant heating rates (CHR) from 2 to 10 °C/min up to 1550 °C and also the corresponding modified heating rates (MHR).

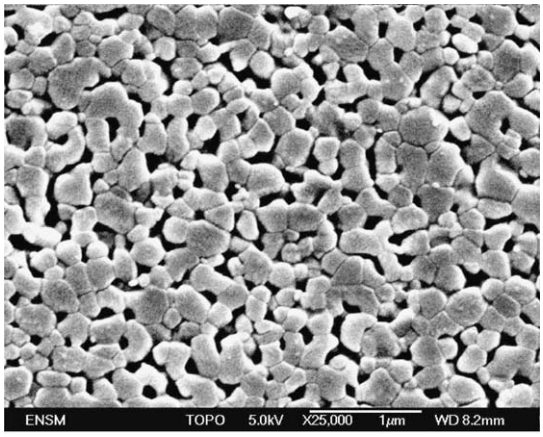

Fig. 14. SEM micrograph of m-C sample heated at 5 °C/min up to 80%.

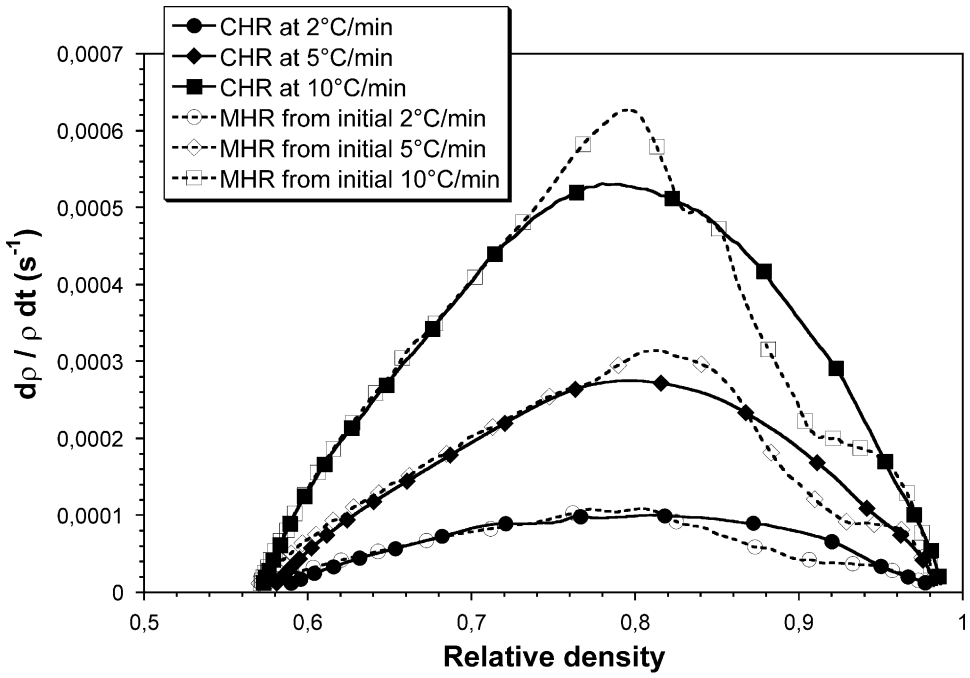

Fig. 15. Densification rate as a function of relative density for m-C2 sample at various constant heating rates from 2 to 10 °C/min up to 1550 °C and also the corresponding modified heating rates.

The increase of heating rate is the same (+40%), whatever the value of the heating rate. The linear part of $\dot{\rho}_i$ has been well extended for MHR samples. Furthermore, a plateau of densification occurs at the end of densification of MHR samples when $\rho > 90\%$, whereas there is no plateau for CHR samples. Fig. 16 show the final microstructures of MHR samples, which respectively come from initial CHR of 2, 5 and 10 °C/min. The onset of abnormal grain growth is observed in the MHR sample from initial 2 °C/min, whereas AGG is very significant in the MHR sample from initial 5 °C/min. In the case of the MHR sample from initial 10 °C/min, a grain size gradient is present [see Fig. 16(c)]. In fact, a high heating rate (higher than 10 °C/min when modified) in a thick sample (10 mm) induces a thermal gradient that produces a grain size gradient. Hence, a new experiment has been performed with a thin sample of 2-mm thickness. Fig. 17 shows the resulting microstructure, which is fine with no size gradient and no AGG. The evolution of $\dot{\rho}_i$ for thick and thin samples is reported in Fig. 18 at MHR from initial 10 °C/min. The evolution of densification is similar for both samples in the beginning of sintering and different at the end. Thus, a plateau of densification occurs between 91 and 96% for thick sample, whereas there is no plateau for thin sample. Therefore, altering heating rate during sintering, in order to extend linearity of $\dot{\rho}_i$, has a great influence on the evolution of densification, especially in the last stage of sintering.

4. Discussion

4.1. Increasing part of densification rate

The striking feature of the data is that the slope of $\dot{\rho}_i = f(\rho)$, at the very beginning of sintering, is constant and independent of green density, whatever the agglomeration state of the alumina powders of this study. There is a distinction between the present work and the study of Rahaman et al.[17] where they showed that green density has a significant effect on the densification rate for ρ values below 80%. However, they studied powder compacts with different green densities, but with the same grain size. Green density alone is not always a reliable indication of pore size. For example, in very agglomerated powders, agglomerates themselves can be very densely packed, leading to high green densities, while still leaving behind large inter-agglomerates pores. Thus, the pore size/particle size ratio is not constant in the study of Rahaman et al.[17] Nevertheless, this ratio is almost constant in the present work, while green densities are different (see Table 2). At the very beginning of sintering, densification behavior is the same, whatever the kind of alumina powders, their agglomeration and their packing state. Therefore, the slope of densification rate is approximately the same at the very beginning of sintering.

Furthermore, the length of the first slope of densification is different according to the kind of sample. In

the case of agglomerate-free sample, such as m-C sample, densification rate increases linearly for 14% of densification. In the case of agglomerated sample, such as a-C sample, densification rate increases linearly for only 3% of densification. For both samples, the initial pore size/particle size ratio is approximately the same; their densification behavior at the beginning of densification is also the same. Thus, both samples have the same areas of equivalent sinterability. These areas of equivalent sinterability are dispersed in a homogeneous way for milled samples and in a heterogeneous way for as-received samples. In the case of a-C sample, the densification of these areas is hindered by agglomerates. It is actually well known that sintering rate decreases with increasing agglomerates content.[21] Furthermore, agglomerates slow down densification and leads to a smaller first slope of densification rate and a second slope of a lower value in the beginning of sintering. Thus, the length of the first slope of densification rate depends on the homogeneity of the green sample. This length for agglomerate-free sample is larger than the one of agglomerated sample. So, the linear behavior of densification rate at the beginning of densification may be used to characterize agglomeration state and packing homogeneity. In the case of m-B sample, a small initial shoulder of densification rate can be attributed to a weak resultant amount of agglomerates. Furthermore, this shoulder disappears after pre-heating treatment. It can be explained by the homogenization of initial microstructure, resulting in a linearly increasing $\dot{\rho}_i$ with relative density.

In addition, the present study showed that temperature derivative of density is independent of heating rate. It has been earlier observed[29] that plots of $d\rho/dT$ as a function of ρ fit a common curve for heating rates from 0.5 to 15 °C/min. The theory of master sintering curve[7] may be used to explain that result. Thus, the authors plotted the following expression for alumina compacts:

$$\ln\left\{\int_0^t \frac{1}{T} e^{-Q/RT} dt\right\} = f(\rho) \quad (5)$$

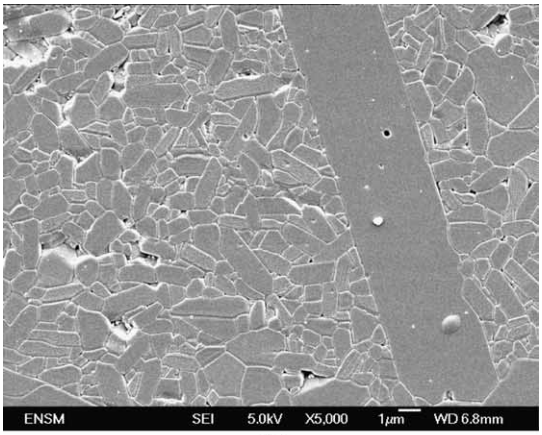

(a)

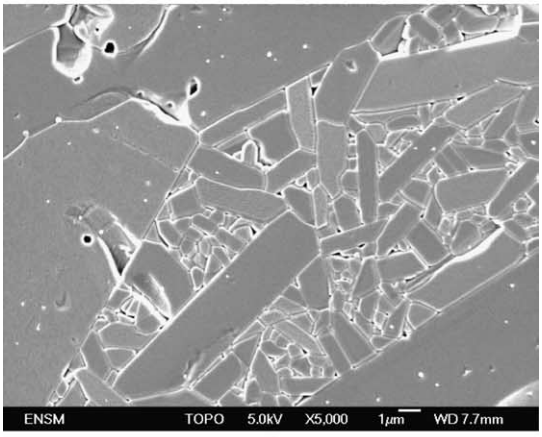

(b)

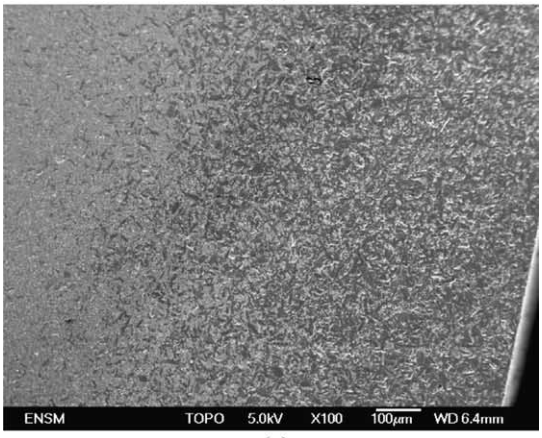

(c)

Fig. 16. (a). SEM micrograph of m-C2 sample sintered up to 1550 °C with modified heating rate from initial 2 °C/min. Final density is 98.7%. (b). SEM micrograph of m-C2 sample sintered up to 1550 °C with modified heating rate from initial 5 °C/min. Final density is 98.9%. (c). SEM micrograph of 10 mm thick m-C2 sample sintered up to 1550 °C with modified heating rate from initial 10 °C/min. Final density is 98.6%.

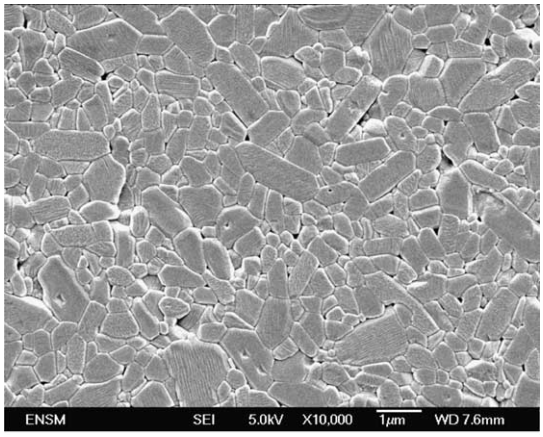

Fig. 17. SEM micrograph of 2 mm thick m-C2 sample sintered up to 1550 °C with modified heating rate from initial 10 °C/min. Final density is 98.9%.

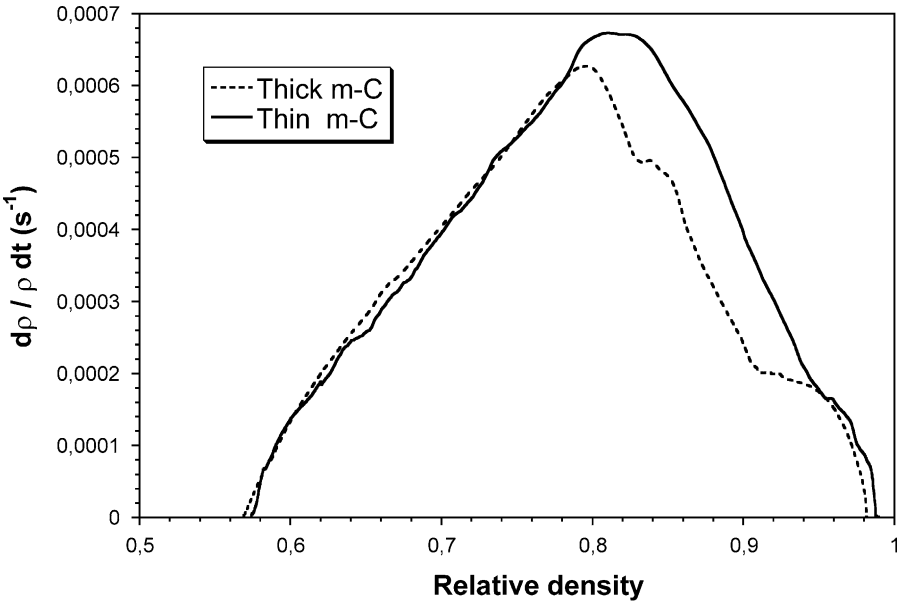

Fig. 18. Densification rate as a function of relative density for thick (10 mm) and thin (2 mm) m-C2 samples sintered up to 1550 °C with modified heating rate from initial 10 °C/min.

They showed that there is a unique curve at any heating rate from 8 to 45 °C/min for $\rho < 96\%$. Following the results of Su et al.,[7] it is therefore possible to write the foregoing expression by integrating with respect to temperature as follows:

$$\ln\left\{\int_0^t \frac{1}{T} e^{-Q/RT} \mathrm{d}t\right\} = \ln\left\{\int_0^T \frac{1}{aT} \mathrm{e}^{-Q/RT} \mathrm{d}T\right\} \quad (6)$$

Here, a is the heating rate. The plot of the right hand side of Eq. (6) as a function of ρ is then independent of heating rate. It is also the same result if the right hand side of Eq. (6) is replaced by the expression $(1/T)(1/a)(\exp(-Q/RT))$. In addition, Eq. (2) can be converted to:

$$\frac{1}{\rho}\frac{\mathrm{d}\rho}{\mathrm{d}T} = AF(\rho)\frac{1}{a}\frac{\mathrm{e}^{-Q/RT}}{T} \quad (7)$$

Assuming that grain size is the same at a constant value of ρ, $AF(\rho)$ function is also the same at a constant value of ρ. Therefore, plots of $\mathrm{d}\rho/\rho\mathrm{d}T$ as a function of ρ are independent of heating rate.

4.2. Maximum densification rate

In an earlier study, Lange[28] studied the sintering of alumina powder compacts at constant heating rates of 2.5 to 20 °C/min up to 1550 °C. He reported that maximum shrinkage rates occurred at the same relative density of 77%, whatever the heating rate. This is in good agreement with the present work, where maximum densification rates occur at the same relative density of about 80%. Here, the resulting microstructure for m-C samples at 80% show porous and dense areas (see Fig. 14). When grain boundaries become linear and leads to produce dense areas, $\dot{\rho}_i$ is slowing down and is moving away from the linear increasing part of densification. When most of the grain boundaries in dense areas are linear, $\dot{\rho}_i$ is maximum. At this maximum, microstructures are the same and independent of heating rate. In addition, the last section showed that plots of $\mathrm{d}\rho/\rho\mathrm{d}T$ as a function of ρ are independent of heating rate. This is also true when heating schedule is altered and whatever the value of the relative density. Therefore, the relative density corresponding to maximum $\dot{\rho}_i$ is not altered, whatever heating schedule.

4.3. Decreasing part of densification rate

Recently, Lim et al.[32] studied the microstructural evolution during sintering of near-monosized agglomerate-free submicron alumina powder compacts. They observed that grain growth is significant when ρ is approximately above 80%. Fig. 19 reports the relative grain size-density trajectories for the samples of the present work. In the case of m-C sample, grain growth is significant when $\rho > 93\%$. In the last part of densification after maximum $\dot{\rho}_i$, coarsening mechanism is promoted. Grain size increases significantly and leads to the decreasing part of densification.

In the present study, a plateau of densification in the last stage of sintering was only observed for heterogeneous m-C2 samples (see Figs. 6 and 15). Furthermore, all samples that undergo this plateau show final microstructure with abnormal grain growth. The main difference between initial powders, that could explain the presence of AGG, is the content of impurities. Thus,

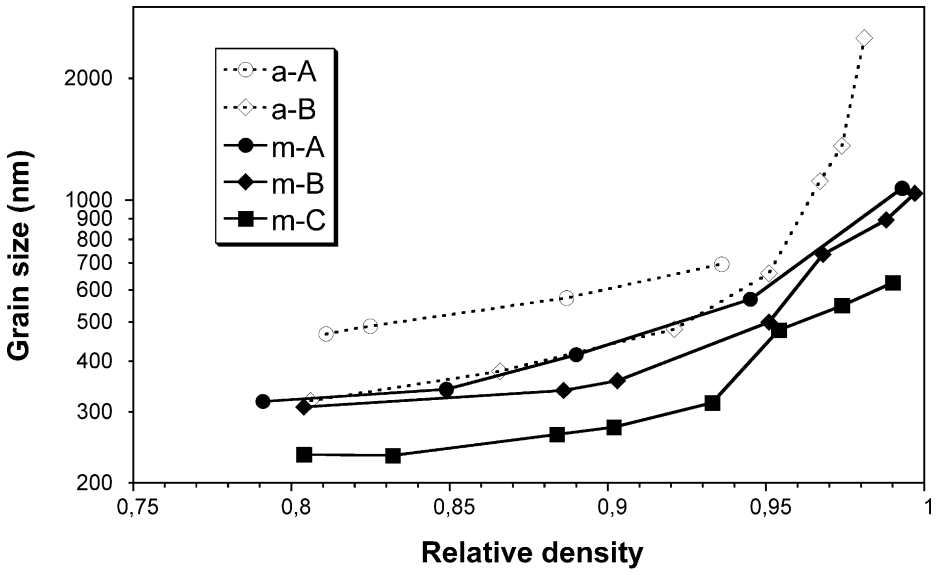

Fig. 19. Grain size-density trajectories for the samples of the present work up to 1550 °C.

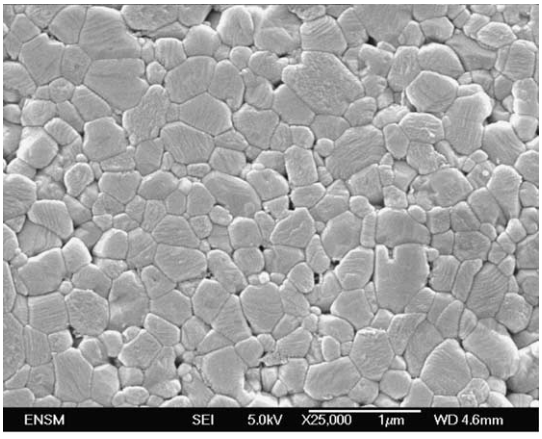

Fig. 20. SEM micrograph of m-C2 sample with modified heating rate from initial 5 °C/min sintered up to 96%.

the silicium impurity content of 132 ppm in C powder is much higher than the one of A and B powders, respectively of 24 and 16 ppm. It is well known that AGG is promoted by the silicium impurity,[33–35] that affects boundary mobility in alumina. In an earlier work, Xue and Brook[36] studied the final stage of sintering of undoped $BaTiO_3$. They observed the existence of an increase in densification rate at the point of onset of AGG. They interpreted it as the result of a favorable pore surface curvature for a pore to be eliminated when it is intersected by an abnormal grain. For example in the present work, a plateau occurs between 93 and 96% of relative density for m-C2 sample sintered with a modified heating rate from initial 5 °C/min. Fig. 20 illustrates the microstructure of that sample at the end of the plateau of densification when $\rho = 96\%$. There is no AGG apparent on the SEM micrograph. This is in discrepancy with the work of Xue and Brook.[36] In addition, the obtained microstructure has no wide particle size distribution and no pores separated from grain boundaries, features which have been recognized as predisposing toward AGG.[37,38] Nevertheless, abnormal grain growth doesn't occur during the plateau of densification, but this plateau indicates the promotion of AGG at the end of sintering.

5. Summary

Densification rate curves as a function of relative density have been investigated on pure alpha alumina under non-isothermal conditions. These curves are sensitive to initial microstructure and heating schedule. They can be correlated with microstructural evolution during overall sintering. The following conclusions were obtained:

- The densification rate, at the very beginning of sintering, is independent of green density and agglomeration state, if initial pore size/particle size ratio is the same.
- In the first part of densification, densification rate increases linearly with one slope if green sample is agglomerate-free, whereas there are two slopes if green sample is agglomerated. The length of the first slope of densification rate depends on the homogeneity of green sample.
- The plots of $d\rho/\rho dT$ as a function of ρ are independent of heating rate.
- In the final stage of sintering, a plateau of densification is observed for heterogeneous green samples and for materials submitted to thermal gradient. Abnormal grain growth is in direct

relationship with this plateau, but doesn't occur during it. The powder packing state of green sample seems to be a main parameter to control abnormal grain growth in the final stage of sintering.

Densification rate curve as a function of relative density is expected to be a good help for choosing raw materials and optimizing heating schedule to monitor microstructural evolution.

Acknowledgements

The authors are grateful to Dr. P. Bowen (EPFL, Switzerland) and Dr. C. Carry (LTPCM, Grenoble, France) for their helpful comments and discussions.

References

1. Young, W. S. and Cutler, I. B., Initial sintering with constant rates of heating. *J. Am. Ceram. Soc*., 1970, **53**, 659–663.
2. Woolfrey, J. L. and Bannister, M. J., Nonisothermal techniques for studying initial-stage sintering. *J. Am. Ceram. Soc*., 1972, **55**, 390–394.
3. Wang, J. and Raj, R., Estimate of activation energies for boundary diffusion from rate-controlled sintering of pure alumina, and alumina doped with zirconia or titania. *J. Am. Ceram. Soc*., 1990, **73**, 1172–1175.
4. Li, J. G. and Sun, X., Synthesis and sintering behavior of nanocrystalline alpha alumina powder. *Acta Mater*., 2000, **48**, 3103–3112.
5. Zeng, W., Gao, L., Gui, L. and Guo, J., Sintering kinetics of alpha Al_2O_3 powder. *Ceram. Int*., 1999, **25**, 723–726.
6. Hansen, J. D., Rusin, R. P., Teng, M.-H. and Johnson, D. L., Combined-stage sintering model. *J. Am. Ceram. Soc*., 1992, **75**, 1129–1135.
7. Su, H. and Johnson, D. L., Master sintering curve: a practical approach to sintering. *J. Am. Ceram. Soc*., 1996, **79**, 3211–3217.
8. Chen, P.-L. and Chen, I.-W., Sintering of fine oxide powders: II, Sintering mechanisms. *J. Am. Ceram. Soc*., 1997, **80**, 637–645.
9. Chen, I.-W. and Wang, X.-H., Sintering dense nanocrystalline ceramics without final-stage grain growth. *Nature*, 2000, **404**, 168–171.
10. Rahaman, M. N., De Jonghe, L. C. and Brook, R. J., Effect of shear stress on sintering. *J. Am. Ceram. Soc*., 1986, **69**, 53–58.
11. Sakarcan, M., Hsueh, C. H. and Evans, A. G., Experimental assessment of pore breakaway during sintering. *J. Am. Ceram. Soc*., 1983, **66**, 456–461.
12. Yan, M. F., Cannon, R. M., Bowen, H. K. and Chowdhry, U., Effect of grain size distribution on sintering density. *Mater. Sci. Eng*., 1983, **60**, 275–281.
13. Zhao, J. and Harmer, M. P., Sintering kinetics for a model final-stage microstructure: a study of Al_2O_3. *Philos. Mag. Lett*., 1991, **63**, 7–14.
14. Zhao, J. and Harmer, M. P., Effect of pore distribution on microstructure development: III, model experiments. *J. Am. Ceram. Soc*., 1992, **75**, 830–843.
15. Slamovich, E. B. and Lange, F. F., Densification of large pores: II, driving potentials and kinetics. *J. Am. Ceram. Soc*., 1993, **76**, 1584–1590.
16. Mayo, M. J., Processing of nanocrystalline ceramics from ultrafine particles. *Int. Mater. Rev*., 1996, **41**, 85–115.
17. Rahaman, M. N., De Jonghe, L. C. and Chu, M.-Y., Effect of green density on densification and creep during sintering. *J. Am. Ceram. Soc*., 1991, **74**, 514–519.
18. Ting, J.-M. and Lin, R. Y., Effect of particle-size distribution on sintering. Part I Modelling. *J. Mater. Sci*., 1994, **29**, 1867–1872.
19. Ting, J.-M. and Lin, R. Y., Effect of particle-size distribution on sintering. Part II sintering of alumina. *J. Mater. Sci*., 1995, **30**, 2382–2389.
20. Evans, A. G., Considerations of inhomogeneity effects in sintering. *J. Am. Ceram. Soc*., 1982, **65**, 497–501.
21. Dynys, F. W. and Halloran, J. W., Influence of aggregates on sintering. *J. Am. Ceram. Soc*., 1984, **67**, 596–601.
22. Hsueh, C.-H., Evans, A. G. and McMeeking, R. M., Influence of multiple heterogeneities on sintering rates. *J. Am. Ceram. Soc*., 1986, **69**, C–64-C-66.
23. Lin, M., Rahaman, M. N. and De Jonghe, L. C., Creep-sintering and microstructure development of heterogeneous MgO compacts. *J. Am. Ceram. Soc*., 1987, **70**, 360–366.
24. Ikegami, T., An apparent sintering mechanism depending on the fabrication history of a powder. *J. Ceram. Soc. Jpn*., 1988, **96**, 1037–1039.
25. Palmour III., H., Huckabee, M. L. and Hare, T. M., Microstructural development during optimized rate controlled sintering. In *Ceramic Microstructure 1976*, ed. R. N. Fulrath and J. A. Parks. Westview Press, Boulder, CO, 1977, pp. 308–319.
26. Harmer, M. P. and Brook, R. J., Fast firing—microstructural benefits. *J. Br. Ceram. Soc*., 1981, **80**, 147–149.
27. Genuist, C. and Haussonne, J. M., Sintering of $BaTiO_3$: dilatometric analysis of diffusion models and microstructure control. *Ceram. Int*., 1988, **14**, 169–179.
28. Lange, F. F., Powder processing science and technology for increased reliability. *J. Am. Ceram. Soc*., 1989, **72**, 3–15.
29. Chu, M.-Y., Rahaman, M. N. and De Jonghe, L. C., Effect of heating rate on sintering and coarsening. *J. Am. Ceram. Soc*., 1991, **74**, 1217–1225.
30. Sato, E. and Carry, C., Effect of powder granulometry and pretreatment on sintering behavior of submicron-grained alpha alumina. *J. Eur. Ceram. Soc*., 1995, **15**, 9–16.
31. Palmour III., H. and Johnson, D. R. In *Sintering and Related Phenomena*, ed. G. C. Kuczynski et al. Gordon and Breach Publishers, New York, 1967, pp. 779–791.
32. Lim, L. C., Wong, P. M. and Ma, J., Microstructural evolution during sintering of near-monosized agglomerate-free submicron alumina powder compacts. *Acta Mater*., 2000, **48**, 2263–2275.
33. Handwerker, C. A., Morris, P. A. and Coble, R. L., Effects of chemical inhomogeneities on grain growth and microstructure in Al_2O_3. *J. Am. Ceram. Soc*., 1989, **72**, 130–136.
34. Bae, I.-J. and Baik, S., Abnormal grain growth of alumina. *J. Am. Ceram. Soc*., 1997, **80**, 1149–1156.
35. Yoo, J. H., Nam, J. C. and Baik, S., Quantitative evaluation of glass-forming impurities in alumina: equivalent silica concentration (ESC). *J. Am. Ceram. Soc*., 1999, **82**, 2233–2238.
36. Xue, L. A. and Brook, R. J., Promotion of densification by grain growth. *J. Am. Ceram. Soc*., 1989, **72**, 341–344.
37. Brook, R. J., Controlled grain growth. In *Treatise on Materials Science and Technology*,Vol. 9, 1976, pp. 331–364.
38. Harmer, M. P., Bennison, S. J. and Narayan, C., Microstructural characterization of abnormal grain growth development in Al_2O_3. *Mater. Sci. Res*., 1983, **15**, 309–320.